Supplementary Material (ESI) for Chemical Communications

ESI supplementary information for Chemical Communications

Monitoring the aluminium coordination during microporous oxide crystallisation by *in situ* soft X-ray absorption spectroscopy

Andrew M. Beale[a], Ad M.J. van der Eerden[a], Didier Grandjean[a], Andrei V. Petukhov[b], Andy D. Smith[c] and Bert M. Weckhuysen*[a]

[a] Inorganic Chemistry and Catalysis, Department of Chemistry, Utrecht University, Sorbonnelaan 16, 3584 CA Utrecht, The Netherlands

[b] van 't Hoff Laboratory for Physical and Colloid Chemistry, Utrecht University, Padualaan 8, 3584 CH Utrecht, The Netherlands

[c] CCLRC Daresbury Laboratory, Keckwick Lane, Daresbury, Warrington, WA4 4AD, UK

Al K-edge NEXAFS data

In figure 1 we show the Al K-edge NEXAFS data recorded for the aluminium source (pseudoboehmite), and the reference material zeolite A (LTA) under hydrated and dehydrated conditions. The edge positions, determined from the maximum in the intensity of the 1st derivative of the spectra, were *ca.* 1568.4 eV ($Al(NO_3)_3.9H_2O$) 1567.8 (pseudoboehmite), 1566.0 (LTA dehydrated) and 1566.9 eV (LTA hydrated) respectively. In addition features at *ca.* 1574.0 could be identified in the $Al(NO_3)_3.9H_2O$ (and 1585.6 eV) and pseudoboehmite spectra (also 1592.7) and features at *ca.* 1573.5 and 1585.6 eV in the remaining others. These white line positions and features were consistent with the presence of tetrahedral Al^{3+} in the dehydrated LTA sample and a distorted octahedral environment in $Al(NO_3)_3.9H_2O$ and pseudoboehmite.[1, 2] A shift in the edge position by + 0.9 eV for the hydrated LTA sample (relative to dehydrated LTA) and an increase in the intensity of the white line was also consistent with the zeolite possessing a mixture of tetrahedral, octahedral and maybe even five coordinated Al^{3+} sites as water binds to some of the Al^{3+}.[2] However the increase in the intensity of the features at *ca.* 1573.5 and 1585.6 eV was more difficult to rationalise. It might be that these features only appeared to be increased due to the effect of heat on the sample causing oscillation damping of the data for the dehydrated sample recorded at 150ºC relative to the hydrated sample measured at room temperature. However it might also be caused by a distortion of some of the tetrahedral Al^{3+} sites due to the interaction with water.

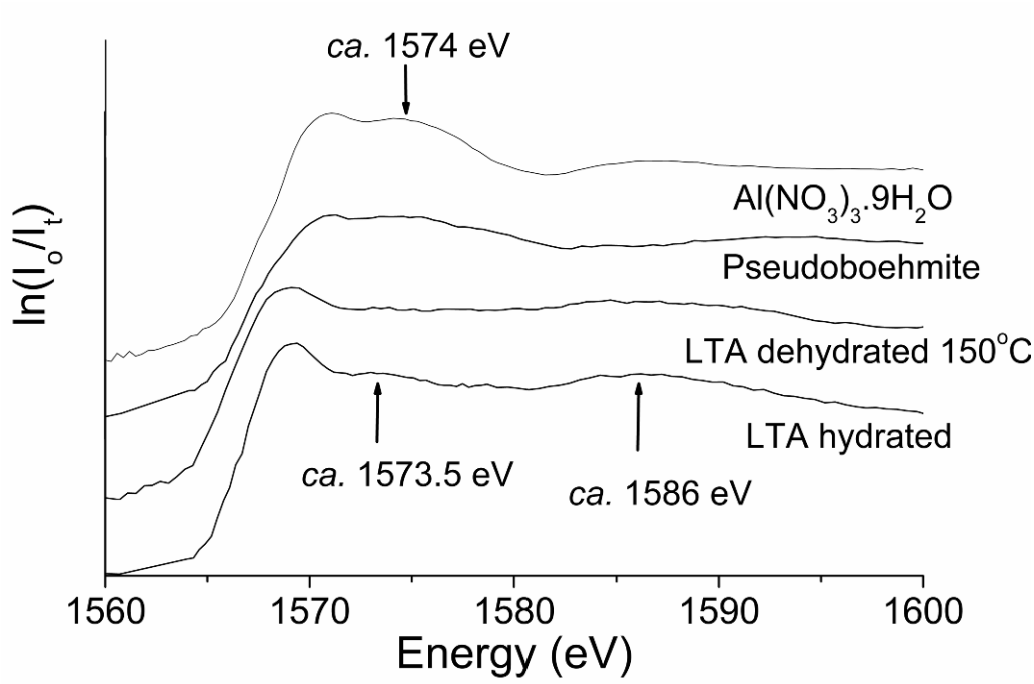

Figure 1. Experimental Al K-edge NEXAFS data for $Al(NO_3)_3.9H_2O$, the aluminium source (pseudoboehmite), and zeolite A (LTA) in a hydrated and dehydrated form. The edge positions determined from the maximum in the 1st derivative of the spectra were 1568.4 ($Al(NO_3)_3.9H_2O$), 1567.8 (pseudoboehmite), 1566.0 (LTA dehydrated) and 1566.9 eV (LTA hydrated) respectively.

Determination of XANES intensities for estimation of coordination states of Al^{3+}

Since it has previously been shown that the height of the rising absorption edge is greater for octahedral complexes than for tetrahedral systems[1] it is possible to obtain a rough estimate for the % age of tetrahedral/octahedral Al^{3+} in the gel/crystalline material (Fig. 3 in the paper) using a linear combination of the intensities of both coordination contributions. For the octahedral Al^{3+} reference we used $Al(NO_3)_3.9H_2O$ and for the tetrahedral Al^{3+} reference the dehydrated LTA sample. This intensity information was then obtained by fitting a Gaussian profile to the XANES region around the maximum of the rising absorption edge. An estimation of error in these data was determined from the standard deviation in the maximum of the X-ray absorption edge intensity from 2 – 3 scans of the sample under identical conditions.

Al K-edge EXAFS data

To demonstrate further the viability of this setup for obtaining SOXAFS data, detailed analysis of the EXAFS (data recorded from 1500 eV to 1850 eV) was also performed.

In order to obtain analysable data with a better signal:noise ratio to allow for a more reliable EXAFS analysis, 2 – 3 scans were recorded for each sample and summed before processing. XAS data were processed using the suite of programs available at Daresbury laboratory, namely EXCALIB (for converting the raw data to energy vs. absorption coefficient), EXBROOK (for background subtraction to extract EXAFS) and EXCURV98 (to extract more detailed local structural details of the catalysts).[3] Data were corrected for self-absorption since they were collected in total fluorescence mode and hence severe amplitude damping was observed. Data were corrected for self-absorption using the ATHENA programme using the ATOMS correction for an infinitely thick sample, which calculates an approximate difference based on tabulated data for absorption coefficients.[4] Corrected data (for S_o^2 & σ^2) were then fitted in k-space (k weighted) between 3.5 and 8.0 $Å^{-1}$ up to a maximum of 3 Å (R-space).

In figure 2 we show the EXAFS data collected for a dehydrated LTA sample at 300ºC in a dry helium atmosphere and the final CoAPO-5 material after the *in situ* crystallisation experiment. The results from this data analysis are given in Table 1. We observed that although the coordination numbers tended to be lower than 4 (which would be expected for tetrahedral Al^{3+} in these samples), an average bond distance close to 1.68 Å (which is a more reliable parameter that can be extracted from EXAFS analysis) is consistent with the presence of tetrahedral Al^{3+} species.[5, 6] The lower coordination numbers obtained for these samples are probably due to self-absorption and the likely difficulties in calculating the extent to which this affects the X-ray data. However these low numbers still remain within the determined error limit for this parameter of ± 1. [7] For the CoAPO-5 hydrothermal sample the average coordination number and bond distance appear to be slightly larger than those determined from the reference dehydrated LTA. This appears to be consistent with the XANES data recorded for this sample in which it appeared that, in comparison to AlPO-5, some of the Al^{3+} species might possess higher coordination or undergo some site distortion.

Table 1. Details extracted from analysis of the EXAFS data shown in Figures 2 and 3.

Materials	R (Å)	N	σ^2/ Å^2	R-factor (%)
$LTA_{(dehyd.)}$	1.68	3.3	0.020	31.0
$CoAPO\text{-}5_{(sample)}$	1.70	3.4	0.023	40.7

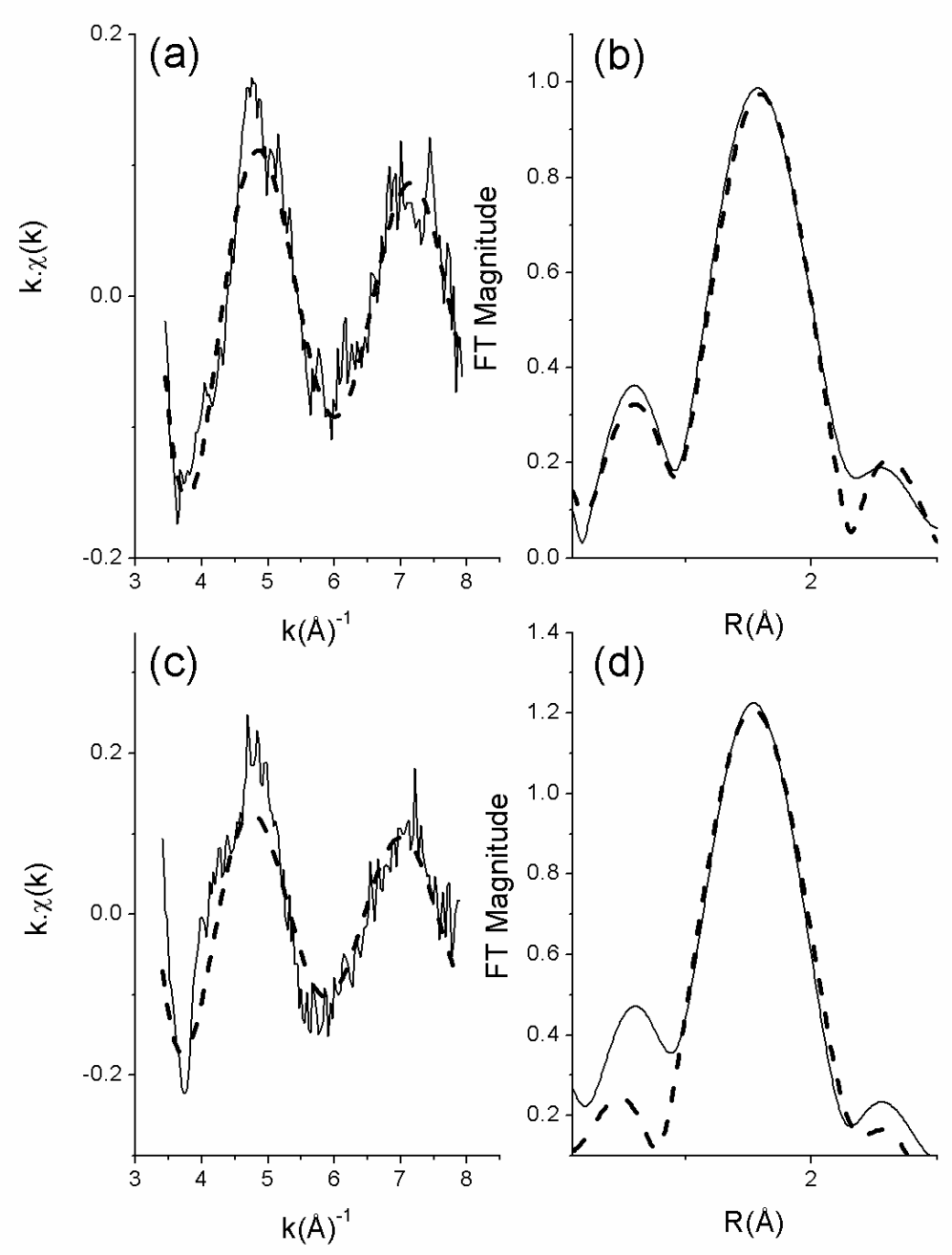

Figure 2. Al K-edge EXAFS data and associated Fourier Transforms (FT's) extracted from a dehydrated zeolite A sample (a) & (b) and hydrothermally crystallised CoAPO-5 (c) & (d). The best fit to the data is illustrated using a dashed line and the results of the analysis given in Table 1.

SAXS/WAXS study of (Me)AlPO-5 crystallisation

A commonly used and powerful technique to study zeolite crystallisation is *in situ* SAXS/WAXS. Despite this it is somewhat surprising that it has rarely been used (with the exception of our recent work and a study by Tiemann et al. on mesostructured aluminophosphate/dodecyl phosphate composite materials)[8, 9] to study AlPO crystallisation. In our recent *in situ* study, the crystallisation of CoAPO-5 was followed using SAXS/WAXS and a number of spectroscopic techniques and it was demonstrated that although the presence of cobalt has a significant influence on the crystallisation process, it also acts as a very valuable probe yielding information on the different stages of the crystallisation process.[8, 10] Here we focus on the similarities of the crystallisation of pure AlPO-5 and CoAPO-5 materials and try to relate the observations here with those seen in the SOXAFS data.

In situ, SAXS/WAXS crystallisation studies were carried out in a cell as previously described.[8] The cell was heated at a rate of one degree per minute from room temperature up to 180°C and remained at this temperature for up to 3 hours under autogeneous pressure and static conditions. For ease of comparison between the different experiments the reaction time t was scaled to the temperature T (1ºC = 1 minute) with t = 0 min corresponding to T = 0ºC. Up to a value of 180 the time and temperature scale are then identical whereas values over 180 only correspond to reaction time. Small and wide-angle scattering data were collected on beamline DUBBLE (BM26B) at the European Synchrotron Radiation Facility (ESRF, Grenoble, France), operating at 6 GeV with a current of 200 mA. The beamline is equipped with a Si (111) double-crystal monochromator. SAXS patterns were measured at a wavelength 1.00 Å using a gas-filled detector (130 × 130 mm^2) positioned at a distance of 1.5 m from the sample corresponding to scattering k vectors in the range $0.3 < k < 6$ nm^{-1}, which gave us access to the first Bragg peak corresponding to the (100) reflection of the AFI structure (11.94 Å). Due to the very small amount of material formed during the reaction, the beam size was reduced to a minimum size (150 μm) and was positioned at the lower part of the cell aperture. A gas-filled WAXS detector positioned at a distance of 1 m was used to record the higher order Bragg reflections of the AFI crystalline structure. The high-intensity

synchrotron radiation allowed us to collect SAXS and WAXS patterns simultaneously with a good signal-to-noise ratio every two minutes. The data were normalised for the intensity of the transmitted X-ray beam thus correcting for the decay of the intensity as well as for sample absorption. Furthermore, a background subtraction was performed using data measured from a cell containing water. For the calibration of the SAXS and WAXS patterns, a silver behenate reference sample and a fully crystallised AlPO-5 material were used respectively.[11-13]

The stacked 3D small-angle log-linear scattering profiles I(k) measured as a function of the crystallisation temperature of AlPO-5 and CoAPO-5 are respectively shown in Figure 3. The onset of crystallisation can be easily observed by the appearance above 150ºC of the Bragg peak at k = 5.26 nm^{-1} corresponding to the (100) reflection of the AFI structure[13] and no pronounced variations in the I(k) profiles were observed to occur at any stage of the crystallization process. However, it is clear that some significant variations of the scattering pattern are appearing more or less concomitantly with the occurrence of the Bragg peak in the low k-range (0.3-2 nm^{-1}). The large fluctuations of the SAXS intensity that appeared after the onset of crystallization are likely to be due to macroscopic movements of the reaction products within the synthesis cell leading to fluctuations of the content of the volume irradiated with the X-ray beam than to real structural changes. This is not an uncommon problem encountered for hydrothermal crystallization of microporous aluminophosphates.[14, 15] Contrary to the work of de Moor et al. carried out on zeolites, no marked feature in the scattering pattern that could be directly linked to the existence of 2.8 nm primary units is visible in our work.

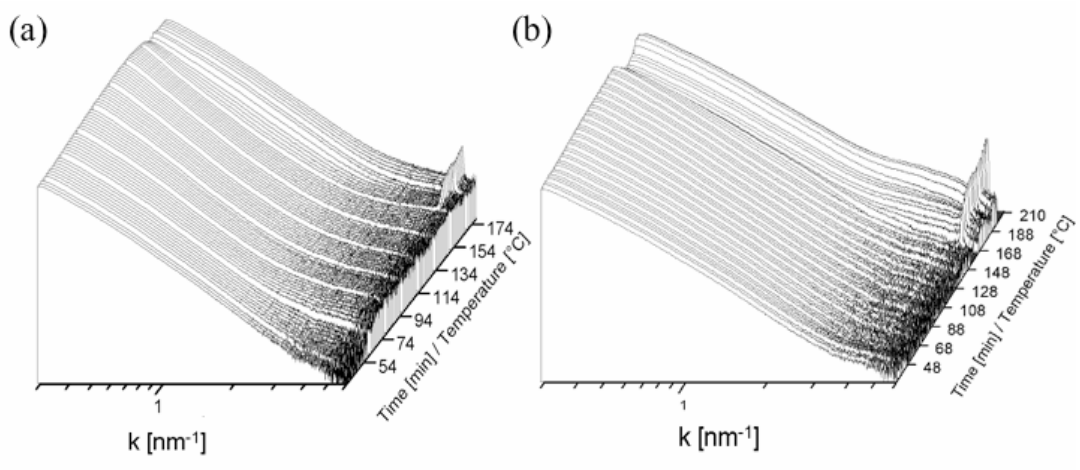

Figure 3. Three-dimensional stack log-log plot of SAXS patterns recorded *in situ* during crystallisation of (a) pure AlPO-5 (b) CoAPO-5 during heating of the precursor gel from room temperature to 180°C. A Bragg peak at k = 5.26 nm^{-1} corresponding to the (100) reflection of the AFI structure was observed at temperatures of 151°C (AlPO-5) and 160°C respectively.

As has been previously observed, the SAXS intensity I(k) closely followed a power-law decay k^{-n} where n ~ 3.[8] Very similar decay has already been observed in various SAXS studies conducted on the crystallization of different types of zeolite indicating that such a spectrum of spatial density fluctuations is common to the precursor gel phase for molecular sieves.[14, 15]

Despite the apparent similarity between the profiles, a detailed analysis shows that small variations can indeed be detected during the various stages of the reaction. Following the procedure developed in our previous work we focus on the k-range from 0.35 to 1 nm^{-1} and remove the leading k^{-3} decay by plotting the $I(k)*k^3$ dependences. The profiles now show a broad maximum, which monotonically shifts to smaller k values with increasing temperature up to the crystallization onset. We have fitted the obtained $k^3*I(k)$ dependences versus $\log_{10}(k)$ to Gaussian profiles. The choice of the Gaussian function is rather arbitrary since any other bell-shaped function could also be used. From the Gaussian fits we have determined the values k_{max} corresponding to the maximum of the $I(k)*k^3$ dependence. The corresponding reciprocal values $2\pi/k_{max}$ for all scattering profiles measured during the crystallization process are plotted as a function of temperature in Figure 4. Surprisingly, the values showed in this figure display very little noise despite the significant uncertainties affecting the original data. At temperatures close to the crystallization onset the

maximum of the $I(k)*k^3$ dependence shifts outside our measurement range leading to a significant increase of the uncertainty of the k_{max} value. Although the data does not provide us with sufficient evidence of the exact nature of the structural transformation in the gel, in our previous work we interpreted k_{max} as the inverse of the typical size of gel aggregates. Therefore we observe that the size of these aggregates would then increase as a function of the temperature from *ca.* 8 nm at room temperature up to a 'maximum' of 40 nm in pure AlPO-5 and up to *ca.* 24 nm in CoAPO-5. However the very broad nature of the Gaussian fits suggests that the size distribution of these aggregates is very large and that k_{max} corresponds only to the center of the distribution curve.

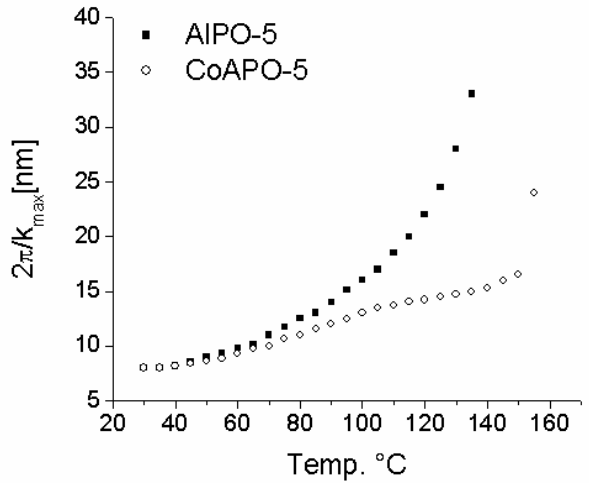

Figure 4. Evolution of $2\pi/k$ maximum as a function of the temperature during the crystallization of pure AlPO-5 and CoAPO-5. Although not shown, it was observed that for CoAPO-5, 8ºC before the occurrence of Bragg peaks the aggregate size is still *ca.* 16 nm whereas the size of the first crystallite was evaluated at *ca.* 42 nm, highlighting the rapidity of the final step of the aggregation.

Comparatively, the two gels show slightly different behavior as a function of the temperature. Although they feature the same approximate aggregate size in the initial gel, in the early stages of the crystallization the growth behaviour starts to diverge as temperatures exceed 60ºC. For the pure AlPO-5 gel the aggregates show a strong temperature dependency since growth accelerates as a function of the reaction temperature. In contrast for the metal substituted samples, aggregation can be described as a two-step process, characterised by a steady increase in size at a constant rate up to a critical point/temperature before rapid growth takes over. This

point corresponded to a particle size of *ca.* 16 nm. It would seem therefore that pure AlPO-5 crystallization seems to proceed very smoothly as a function of the temperature whereas the crystallization of CoAPO-5 showed a more contrasted evolution.

Crystalline Bragg peak analysis

The intensity of the (100) Bragg peaks at k = 5.26 nm^{-1} seen in the SAXS data shown in Figure 5 were observed to increased with time until a maximum was reached after *ca.* 40 min into the crystallisation of all samples. The evolution of diffraction peak intensity as a function of time can be used to derive information on the kinetics and the mechanism involved in the crystallization process. The intensity of the Bragg reflections as a function of time was determined by fitting the peaks with a Gaussian function and converted to an extent of reaction (α), scaled from 0 to 1, using the relationship α (t)= $I_{hkl}(t)/I_{hkl}(max)$, where $I_{hkl}(t)$ is the area of a given peak at time t, and $I_{hkl}(max)$ the maximum area of this peak.

Table 2. Details extracted from analysis of the WAXS data and Sharp-Hancock plots in Figure 6 for the crystallisation of pure and cobalt substituted (Me)AlPO-5 materials.

Materials	Temperature of the onset of crystallisation [°C]	First measurable crystallite size [nm]	End crystallite size [nm]	n-factor [a.u.]	k-factor [s^{-1}]
AlPO-5	151	42	58	1.02	$2.00\ 10^{-3}$
CoAPO-5	160	40	63	1.50	$6.55\ 10^{-4}$

The integration of this reflection and the evolution of the change in its full-width at half maximum (FWHM) for CoAPO-5 and the pure AlPO-5 materials are shown in Figure 5. The resultant crystallisation curves were typical for AlPO crystallisation[16] and consist of an induction period followed by crystallisation and at first rapid growth of the AFI structure, which slows as the nutrients for growth are consumed. This behaviour is more clearly observed in the FWHM plots, which were observed to decrease rapidly up to a point that coincided with the change in rate of the reaction and remained relatively constant until the extent of the reaction reaches its maximum

value. The corresponding values of the crystallite size at the onset of crystallisation are shown in Table 2. It is interesting to note that the first measurable crystallite size during the onset was *ca.* 40 nm and at the end of crystallisation was *ca.* 60 nm for all samples.

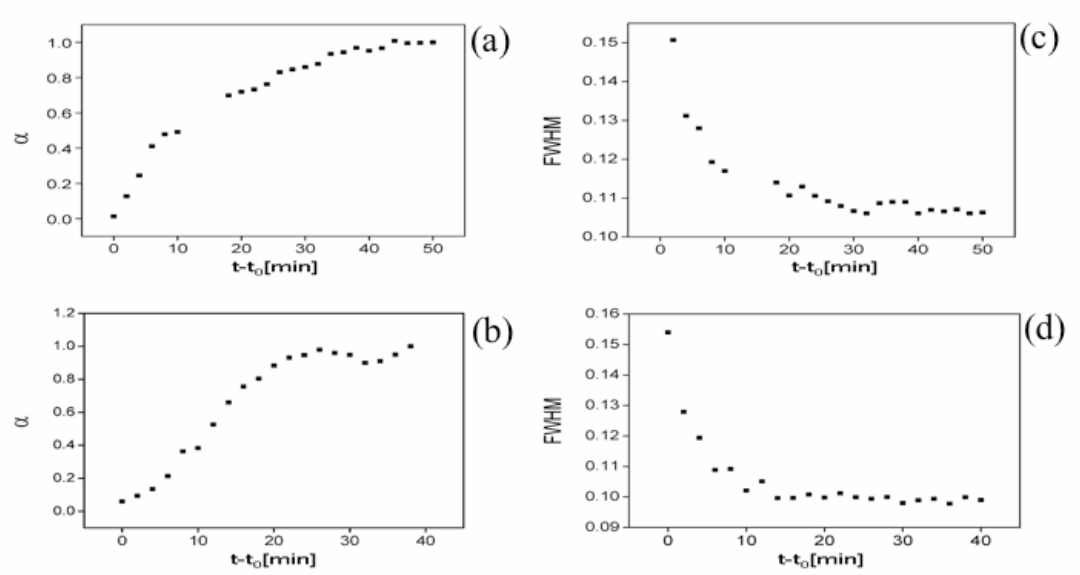

Figure 5. Extent of reaction plots for the crystallisation of (a) AlPO-5 and (b) CoAPO-5 using the experimental integrated values of the (100) reflection for the AFI structure observed in the SAXS detector at 11.94 Å to determine the extent of the reaction as a function of time (t_0 corresponds to the onset of crystallisation). In (c) and (d) are shown the evolution of the experimental full width at half maximum (FWHM) values of the same reflection.

Kinetic information on the crystallisation process can be derived from the Avrami-Erofe'ev[17-20] expression that is widely used to model phase transitions and crystal growth in solid-state chemistry using the extent of the reaction, α, to time t using the relationship:

$$\alpha=1-\exp[-(k(t-t_0))^n]$$

where t is the induction time, k the rate constant, and *n* is the Avrami exponent. The exponent *n*, can be used in most cases to deduce information about the rate of nucleation and the mechanism of growth. Common values of *n* ranges from n = 0.5 to n = 4 and contain information both on the dimensionality and the process of crystallisation.[21] Previous work has demonstrated the relevance of this equation in modelling a variety of solid-state reactions but showed that this expression is found to

be most applicable in the range $0.15 < \alpha < 0.8$. A Sharp-Hancock plot (ln [-ln(1-α)] v. ln (time)) was used to obtain the gradient *n* and intercept *n* ln k.[22] The resultant plots for the crystallisation of both samples are presented in Figure 6 and were clearly linear over the whole extent of the data confirming the validity of the model. (Outliers due to the occurrence of macroscopic inhomogeneities in the sample during the synthesis were not included in the linear fitting process). The corresponding *n* and k parameters derived respectively from the gradient and the intercept of the lines fitted by linear regression for the CoAPO-5 sample and pure AlPO-5 are displayed in Table 2.

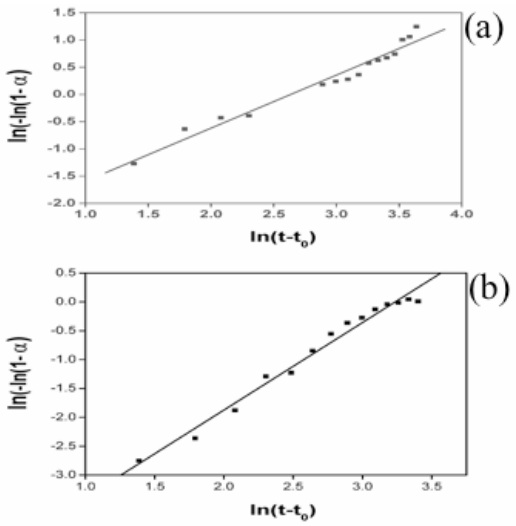

Figure 6. Sharp-Hancock plots for (a) AlPO-5 and (b) CoAPO-5 plotted over the data range $0.15 < \alpha < 0.80$

A similar trend to the crystallisation onset temperature was observed for the derived values of the rate constants (k) with pure CoAPO-5 presenting the slowest rate. This difference suggested that the crystallisation process is affected by the nature of the metal ion to be incorporated in the aluminophosphate network.

Interpretation of the value of the *n* factor obtained from the Avrami plots is more difficult since the same value may correspond to different theoretical mechanisms. However a value of $n = 1$ obtained for pure AlPO-5 is most likely to correspond to a diffusion controlled one-dimensional growth with a decreasing nucleation rate. In the case of CoAPO-5 the higher value for the *n* parameter (*ca.* 1.5) indicated that it most likely that the material crystallises with the same dimensionality as the pure AlPO-5

but that the crystallisation mechanism was shifting from a diffusion-limited to phase-boundary limited growth. As was shown the crystallisation of CoAPO-5 is both slower and occurs some *ca.* 10°C higher than the pure AlPO-5 as Co^{2+} has to first change its coordination state from six to four-fold before crystallisation begins.

References

1 J. A. van Bokhoven, H. Sambe, D. E. Ramaker, and D. C. Koningsberger, *J. Phys. Chem. B*, 1999, **103**, 7557.
2 J. A. van Bokhoven, A. M. J. van der Eerden, and D. C. Koningsberger, *J. Am. Chem. Soc.*, 2003, **125**, 7435.
3 N. C. Binsted, J. W. Campbell, S. J. Gurman, and P. C. Stephenson, *EXAFS Analysis Programs, Daresbury Laboratory, Warrington*, 1991.
4 B. Ravel and M. Newville, *J. Sync. Rad.*, 2005, **12**, 537.
5 I. J. Drake, Y. Zhang, M. K. Gilles, C. N. Teris Liu, P. Nachimuthu, R. C. C. Perera, H. Wakita, and A. T. Bell, *J. Phys. Chem. B*,, 2006, **110**, 11665.
6 J. A. van Bokhoven, J. Roelofs, K. P. de Jong, and D. C. Koningsberger, *Chem. Eur. J.*, 2001, **7**, 1258.
7 P. A. O'Day, J. J. Rehr, S. I. Zabinsky, and G. E. Brown, *J. Am. Chem. Soc.*, 1994, **116**, 2938.
8 D. Grandjean, A. M. Beale, A. V. Petukhov, and B. M. Weckhuysen, *J. Am. Chem. Soc.*, 2005, **127**, 14454.
9 M. Tiemann, M. Froba, G. Rapp, and S. S. Funari, *Chem. Mater.*, 2000, **12**, 1342.
10 B. M. Weckhuysen, D. Baetens, and R. A. Schoonheydt, *Angew. Chemie.*, 2000, **39**, 3419.
11 T. C. Huang, H. Toraya, T. N. Blanton, and Y. Wu, *J. App. Cryst.*, 1993, **26**, 180.
12 T. N. Blanton, C. L. Barnes, and M. Lelental, *J. App. Cryst.*, 2000, **33**, 172.
13 G. J. Klap, H. van Koningsveld, H. Graafsma, and A. M. M. Schreurs, *Microp. Mesop. Mater.*, 2000, **38**, 403.
14 P. de Moor, T. P. M. Beelen, R. A. van Santen, K. Tsuji, and M. E. Davis, *Chem. Mater.*, 1999, **11**, 36.
15 P. de Moor, T. P. M. Beelen, and R. A. van Santen, *J. Phys. Chem. B*, 1999, **103**, 1639.
16 G. Muncaster, A. T. Davies, G. Sankar, C. R. A. Catlow, J. M. Thomas, S. L. Colston, P. Barnes, R. I. Walton, and D. O'Hare, *Phys. Chem. Chem. Phys.*, 2000, **2**, 3523.
17 M. Avrami, *J. Chem. Phys.*, 1939, **7**, 1103.
18 M. Avrami, *J. Chem. Phys.*, 1940, **8**, 212.
19 M. Avrami, *J. Chem. Phys.*, 1941, **9**, 177.
20 B. V. Erofe'ev, *C. R. Dokl. Acad. Sci. URSS*, 1946, **52**, 511.
21 S. F. Hulbert, *J. Br. Ceram. Soc.*, 1969, **6**, 11.
22 J. H. Hancock and J. D. Sharp, *J. Am. Ceram. Soc.*, 1972, **55**, 74.